

# Sequence of neurofibrillary changes in aging and Alzheimer's disease: A confocal study with phospho-tau antibody, AD2

M. Galván<sup>a</sup>, J.P. David<sup>b</sup>, A. Delacourte<sup>b</sup>,  
J. Luna<sup>a</sup> and R. Mena<sup>a,\*</sup>

<sup>a</sup>*Departamento de Fisiología, Biofísica y Neurociencias, CINVESTAV-IPN, PO Box 14-740, 07000, México, D.F., México*

<sup>b</sup>*Unité INSERM 422, Place de Verdun, 59045 Lille, Cedex, France*

In the present study, neurons of the entorhinal cortex, hippocampus and frontal lobe from non-demented and Alzheimer's disease (AD) cases, were stained in order to study neurofibrillary changes. We have used double immunolabeling with a phosphorylation dependent monoclonal antibody (mAb) to tau, AD2, and the histochemical dye thiazin red (TR). MAb AD2 specifically recognizes phosphorylated Ser396 and Ser404, while TR shows binding sites for amyloid- $\beta$  and tau when they are in fibrillar states. We show a morphological sequence of changes in the development of neurofibrillary tangles (NFTs), starting from mAb AD2 diffuse labeling in non-NFT bearing cells recognized by mAb AD2, then going through two subtypes of intracellular NFTs, to a final stage as extracellular-NFTs. Morphometric analysis of the density of AD2 immunoreactive structures showed the NFT density in hippocampus and frontal lobe were the best parameters to differentiate normal aging from AD. Densities of AD2 immunoreactive structures in hippocampus and frontal lobe correlated with the Clinical Dementing Rating score. Based upon the variety of appearances of immunoreactivity displayed by mAb AD2, we were able to stage neurofibrillary changes at the level of individual neurons and brain areas. Our results demonstrate that the intensity of neurofibrillary changes in the hippocampus as well as the extent of the degeneration process in association areas differentiate normal aging from AD, and are well correlated with cognitive impairment.

**Keywords:** AD2, Alzheimer disease, confocal microscopy, hippocampus, hyperphosphorylated tau protein, neurofibrillary tangles

## 1. Introduction

The classic histopathological hallmarks of Alzheimer disease (AD) are neurofibrillary tangles (NFTs) and senile plaques. The neurofibrillary pathological structures are first seen in limbic cortical areas, then spread in a predictable, non-random way across the isocortical brain areas [6,26,34,38]. Their density in isocortical areas has been related to the cognitive impairment observed in AD [1,3,15,16]. In AD, NFT formation is associated with neuronal loss [12,23,24] and there is a strong correlation between neuronal degeneration and the transition between intracellular and extracellular NFTs [8]. In addition, it is generally assumed that extracellular NFTs presumably represent neuronal death [12,21,23,24].

Hyperphosphorylated tau proteins are the major antigenic components of paired helical filaments (PHF), which form NFTs, dystrophic neurites in neuritic plaques and neuropil threads [13,22,25,31]. Therefore, phosphorylation of tau protein has been considered an important event of PHF formation. Phosphorylation dependent antibodies were suited to study the gradual development of neurofibrillary structures [2,5,17] as well as to identify the phosphorylated sites that presumably are important in PHF assembly [4,32]. Based on immunocytochemical preparations, Kimura et al. [28] studied the changes in tau phosphorylation state with NFT development. These authors found that phosphorylation of sites Ser199, Ser202, Ser409 and Ser422 occurs early in NFT development and these sites remain phosphorylated throughout later stages of neurodegeneration. Tau protein sites Thr231 and Ser396 may also be phosphorylated in the more advanced stages of NFT formation [28].

---

\*Corresponding author. Tel.: +52 574 73800 ext. 5130; Fax: +52 574 77105; E-mail: rmena@fisio.cinvestav.mx.

Monoclonal antibody AD2 (mAb AD2) recognizes phosphorylation on Ser396 and to a lesser extent on Ser404 [11]. This antibody detects a phosphorylation event that seems to be of great importance for microtubule assembly [19] and for all types of tau pathology [10]. Using confocal microscopy, we have analyzed the immunochemical characteristics of mAb AD2 at different stages of NFT formation that are detected by thiazin red [29,30]. Our confocal analysis provides further support that mAb AD2 is an useful immunocytochemical probe to define the pathological phosphorylation processing of PHF-tau protein.

In this report, we have examined the distribution of mAb AD2 immunoreactive NFTs in different brain areas of well-characterized AD and control patients. The NFT densities were correlated with the Clinical Dementia Rating (CDR) score, a clinical parameter of cognitive state [27]. Our findings support that the extent of neurofibrillary changes associated with abnormally phosphorylated tau protein in the hippocampus and neocortical areas correlate with cognitive impairment in AD.

## 2. Materials and methods

### 2.1. Subjects

Brains were obtained at autopsy (postmortem delay: 7–48 h). Tissue was fixed by immersion in buffered 10% formalin for at least three weeks. 10 demented cases age 69 to 92 (mean  $85 \pm 7$  years) diagnosed as AD and 10 non-demented patients age 63 to 93 (mean  $83 \pm 10$  years) were included. Clinical, neuropathological, and biochemical data for these cases have been previously reported [14]. Briefly, brains for AD patients diagnosed according to NINCDS-ADRDA criteria, were neuropathologically evaluated according to CERAD criteria. Cognitive status was retrospectively evaluated with the Clinical Dementia Rating (CDR) score [27]. The CDR values are as follows: 0 = no memory loss, 0.5 = questionable, 1 = mild, 2 = moderate and 3 = severe dementia. Six of the non-demented group had a CDR of 0. The other four cases had a CDR of 0.5, however, did not conform to CERAD criteria for AD diagnosis. The number of AD cases, by increasing index of severity, were: 1 at 1; 3 at 2; and 6 at 3. The patient with CDR score at 1 was diagnosed as an early or preclinical AD.

### 2.2. Immunocytochemistry

Paraffin-embedded 8  $\mu\text{m}$ -thick sections were obtained from entorhinal cortex, hippocampal formation and frontal cortex Brodman area 9 (BA9) regions of each case. Prior to immunolabeling, sections were incubated with 0.5% hydrogen peroxide in phosphate buffered saline (PBS), pH 7.4, for 30 min. Sections were then incubated overnight, at 4°C, with the mAb AD2, diluted 1:500 in PBS containing 0.2% Triton X-100. An anti-mouse IgG coupled with horseradish peroxidase was used as secondary antibody. Visualization of immunoreactive products was achieved by the peroxidase catalyzed reaction of 0.06% diaminobenzidine with  $\text{H}_2\text{O}_2$ . The reaction was stopped by immersion of the slide in PBS and sections were counterstained with cresyl violet, then dehydrated and coverslipped in DPX mounting medium (Electron Microscopy Sciences, Washington). Control sections were processed in which the primary antibody was omitted. In control preparations, no immunoreactive structures were detected.

### 2.3. Confocal microscopy

Selected sections from the hippocampus were double-labeled with mAb AD2 and the dye thiazin red (TR; Fluka, Busch). After incubation with mAb AD2, overnight at 4°C, sections were then incubated with FITC-tagged goat anti-mouse IgG, at room temperature for 1 h. Sections were counterstained with TR (0.001% in water) for 7 min, washed and mounted in anti-queching media (Vectashield, Vector Labs). TR is a red fluorescent dye that has staining properties similar to thioflavin S [36]. It has been extensively used in our laboratory to differentiate between fibrillar and non-fibrillar states of aggregation of PHF-associated tau protein [29,30]. The double-labelled slides were viewed with a x60 (NA 1.4) oil immersion objective on a Nikon microscope with attached confocal system (Bio-Rad MRC 600, Watford, UK). Sections were excited with green (blue exciter filter, 418 nm) and red (green exciter filter, 514 nm) for mAb AD2 and TR, respectively. From each area, 5–15 serial optical Z-sections (0.2–0.5  $\mu\text{m}$  thick) were collected using the dual channel image system. Data were stored on rewritable optical disk cartridges. The criteria to identify TR-positive intracellular NFTs was based upon tightly-arranged tangles and the presence of a black rounded hole, corresponding to the nuclear space. Likewise, TR-positive extracellular NFTs were defined on the bases of a loosely-arranged tangles in the absence of nuclei and associated lipofuscin granules.

## 2.4. Morphometry and statistics

The density of intracellular NFTs was determined by counting three different fields randomly chosen in each region. The fields of the hippocampus formation were counted as the: CA3-CA2 and CA1-subiculum. Entorhinal cortical layers II and IV were considered together. Polymodal association cortex of BA9 in the frontal cortex was considered alone. Counting was made using a 20x objective lens. The density of AD2-immunoreactive intracellular NFTs was expressed as the number of structures per mm<sup>2</sup>. Data were compiled and processed using standard software. The comparisons between 10 AD and 10 non-demented cases were made using the t-student test. Demented and non-demented cases were considered in the analysis of the correlation between density of intracellular NFTs and CDR score using the Spearman's r coefficient.

## 3. Results

### 3.1. Double labelling with mAb AD2 and thiazin red in the hippocampus

#### A. Neurons devoid of NFTs

Both in control cases and AD, pyramidal neurons with morphological normal appearance which were present in the hippocampus, mainly in CA1 and subiculum, exhibited perinuclear (arrow in Fig. 1(a)) and cytoplasmic diffuse granular mAb AD2 immunoreactivity (arrows in Fig. 1(b)). These mAb AD2 immunoreactive deposits were, in general, not detected with TR, suggesting a non fibrillar state of the first neuropathological changes related to mAb AD2 antigen (Figs 1(b) and 3(B)). However, in some non NFT-bearing neuronal cells the mAb AD2 immunoreactivity that was found in association with endogenous membranes colocalized with TR, while no traces of AD2 immunoreactivity were observed within the karyoplasm (Figs 1(a) and 3(A), arrow). MAb AD2 immunoreactivity was frequently observed mingled with autofluorescent lipofuscin granules located in the cytoplasmic compartment (arrowhead in Figs 1(a) and 3(A); arrows in Figs 1(b) and 3(B)).

#### B. Intracellular-NFTs

Intracellular-NFTs were immunolabeled with mAb AD2. Using double labeling confocal microscopy with this antibody and TR, the fibrillar state of aggregation of AD2 immunoreactive products was analyzed in

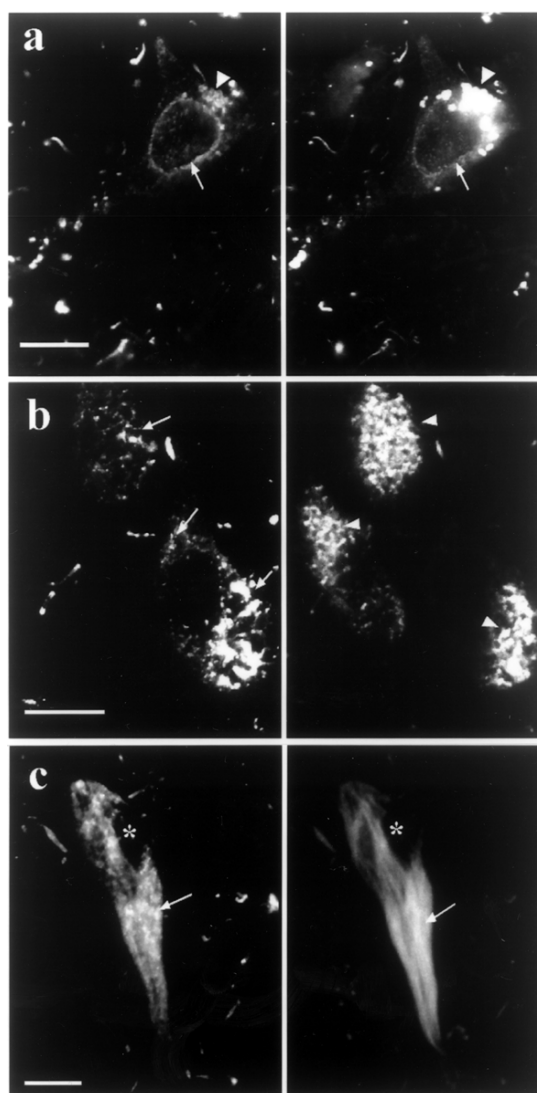


Fig. 1. a–c Double labeling with mAb AD2 and TR in AD brains. (a) a Patchy perinuclear mAb AD2 immunoreactivity is observed in the green channel (left side, arrow) that is faintly detected by TR in the red channel. A fraction of the autofluorescent lipofuscin granules located on the vicinity of the nucleus is also detected by mAb AD2 (arrowhead). (b) Granular mAb AD2 immunoreactivity (arrows) was observed mingled with lipofuscin granules deposits (arrowheads) which are detected in the red channel. Asterisks correspond to the nuclei of the cells. (c) An intracellular tangle that is detected by TR in the red channel displays a mAb AD2 immunoreactivity that takes the form of dense amorphous granular material distributed in patches along the structure (left side, thick arrow). The immunoreactive deposits observed toward the upper part of the cells is not TR associated (left side, thin arrow). The nucleus of the cell appears as a black hole (asterisk). Scale bars = 10  $\mu$ m.

these tangles. This approach evidenced two consistent subtypes of intracellular-NFTs (Figs 3(C) and (D)). As Fig. 1(c) shows, the somatic compartment of neu-

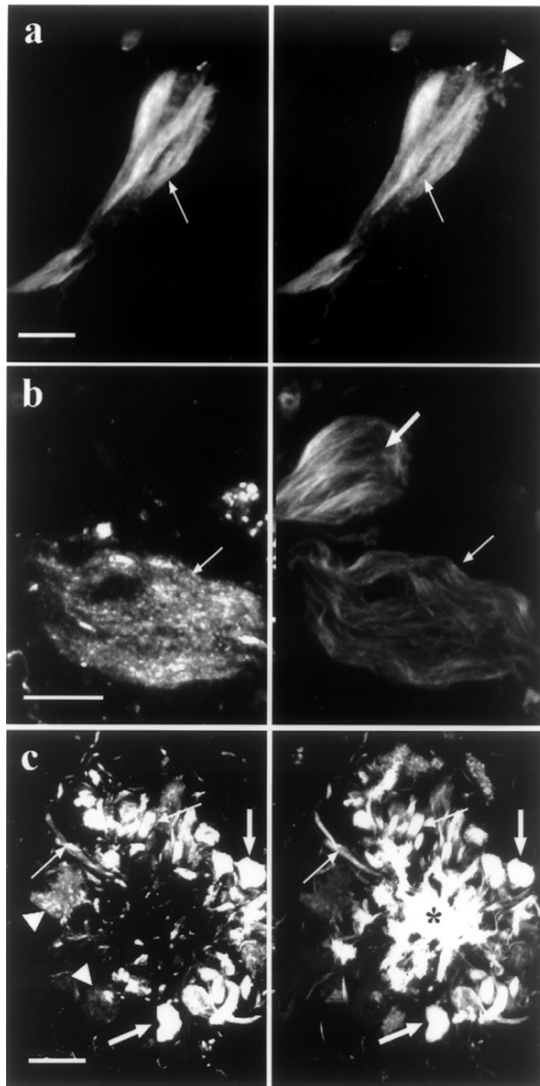


Fig. 2. a–c Double labeling with AD2 and TR. (a) A typical intracellular-NFT (arrow) is double labeled with mAb AD2 in the green channel (left side) and TR (right side) in the red channel. Autofluorescent lipofuscin granules deposits are only observed in the red channel (arrowhead). (b) Extracellular NFT located in the upper part of the image is only detected by TR in the red channel (thick arrow). The extracellular-NFT located in the lower part of the image displayed a residual coarse granular mAb AD2 immunoreactivity (thin arrow). (c) Dystrophic neurites associated with a neuritic plaque whose core is constituted by amyloid- $\beta$  deposits (asterisk) displayed a heterogeneity in both shapes and patterns of immunolabeling with mAb AD2. Large and round neurites were either double labeled with the two markers (thick arrows) or identified only by mAb AD2 (arrowheads). The long and slender neurites were double labeled with mAb AD2 and TR (thin arrows). Scale bars = 10  $\mu$ m.

ronal cell displayed the first subtype of intracellular-NFTs that was characterized by granular mAb AD2 immunoreactivity (Fig. 1(c) left) and positive labeling by

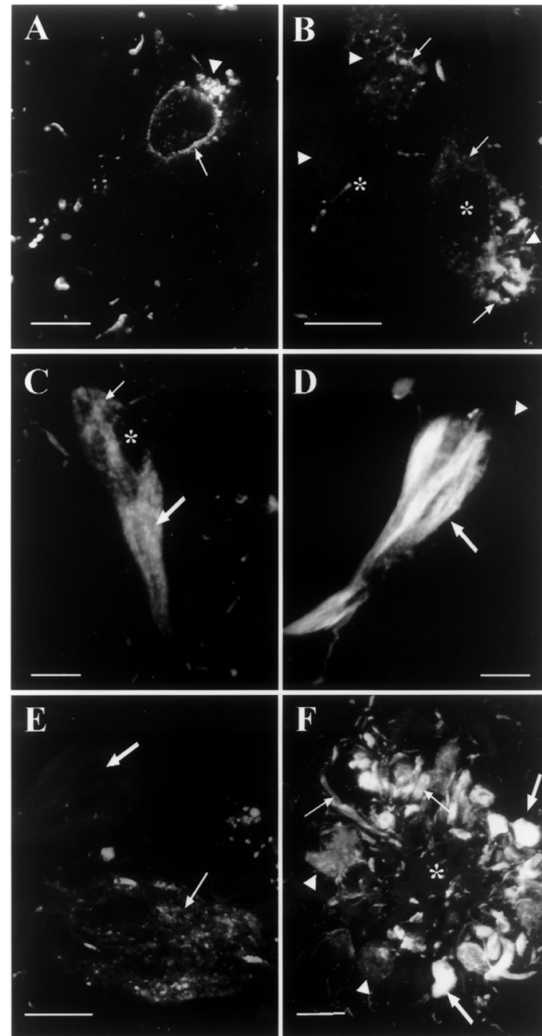


Fig. 3. A Merged color image corresponding to Fig. 1(a) for double labeling AD2 and TR. B Merged color image corresponding to Fig. 1(b). C Merged color image corresponding to Fig. 1(c). D Merged color image corresponding to Fig. 2(a). E Merged color image corresponding to Fig. 2(b). F Merged color image corresponding to Fig. 2(c). Scale bars = 10  $\mu$ m.

TR (Fig. 1(c), right). When both channels were merged the spatial relation between mAb AD2 granular immunoreactivity in green color and PHFs detected by TR in the red channel was observed unevenly distributed along the cytoplasmic surface of the cell (Fig. 3(C)).

The second subtype of intracellular-NFTs was the typical NFT. This lesion was characterized by double labeling of fibrillar appearance which was evident in both channels (Fig. 1(d), left and right arrows). The merged image showed the colocalization (in yellow color) between mAb AD2 fibrillar immunoreactivity and TR (Fig. 3(D)). This differential mAb AD2 labeling

found in these two subtypes of tangles may reflect the state of aggregation of hyperphosphorylated tau in the intracellular-NFTs. For all the cases studied, the second subtype of intracellular-NFTs was the prevalent form of tangles.

### C. Extracellular-NFTs

It has been established that PHF-associated tau protein from intracellular-NFTs, during their transition to the extracellular space to become a "ghost", lose its whole amino terminus and portions of the carboxyl terminus [9,18]. In double labeling mAb AD2 and TR, we identified two subtypes of extracellular NFTs whose differences appeared to be related to the degree of proteolysis in the extracellular space. In subtype 1 extracellular-NFT, illustrated in Fig. 2(b) (thin arrow), mAb AD2 immunoreactivity took the form of granular material (green channel) distributed in "patches" along the surface of the loosely-arranged tangle detected by TR in the red channel (Figs 2(b) and 3(E), thin arrow).

We have called subtype 2 extracellular-NFTs those which appear to be highly degraded. These NFTs have lost all traces of antigenicity for mAb AD2 and are only detected by TR in the red channel (Figs 2(b) and 3(E), thick arrow).

### D. Dystrophic neurites and neuropil threads

The large amounts of dystrophic neurites present in neuritic plaques allowed us to better analyze the different subtypes of such structures as detected by mAb AD2 (Fig. 3(F)). We were able to identify a heterogeneity of immunoreactive dystrophic neurites based upon their size, shape, degree of immunoreactivity and differential distribution. The majority of mAb AD2 immunoreactive neurites associated with the amyloid- $\beta$  fibrillar deposits detected by TR in the red channel (Figs 2(c) and 3(F), asterisk) were large and round (Fig. 3(F)). Some of these enlarged neurites were double labeled by mAb AD2 and TR (Figs 2(c) and 3(F), thick arrows) while some other presented a granular pattern of mAb AD2 immunoreactivity rather than fibrillar and were undetected by TR (Figs 2(c) and 3(F), arrowheads). These patterns of labeling suggest differential states of phosphorylated tau aggregation. Large and round neurites associated to amyloid plaques were observed mainly in molecular layer of the dentate gyrus, CA1 and subiculum regions. Conversely to the latter neurites, long and slender neurites distributed in the neuropil could be associated or not to amyloid- $\beta$  deposits. These neurites were mAb AD2 immunoreactive and double labeled by TR (Figs 2(c) and 3(F), thin arrows). This kind

of neurites when observed randomly distributed in the neuropil did not present any preferential location in the areas studied but were particularly abundant in the most severe cases of AD.

### 3.2. Densities of mAb AD2 immunoreactive structures in AD and non demented control cases

When we quantified the number of mAb AD2 immunoreactive cells displaying the perinuclear and cytoplasmic diffuse patterns both in AD and control cases by areas, non statistical difference was found.

The quantification of mAb AD2 immunoreactive intracellular-NFTs in CA3-CA2 ( $P = 0.003$ ), CA1-subiculum ( $P < 0.0001$ ), entorhinal cortex ( $P = 0.0009$ ) and BA9 ( $P = 0.008$ ), revealed that their density were significantly different between AD and non-demented groups (Fig. 4). In AD cases the highest density of intracellular-NFTs was found in the CA1-subiculum region, followed by entorhinal cortex, BA9 in the frontal cortex and in CA3-CA2 areas in the hippocampus. Control cases did not show this distribution pattern (Fig. 4).

### 3.3. Correlation between tangles and CDR

No correlation was found between the density of mAb AD2 immunoreactive cells displaying the perinuclear and cytoplasmic diffuse patterns and cognitive impairment among the cases studied.

On the other hand, the density of mAb AD2 immunoreactive intracellular-NFTs in the 20 cases correlated with the cognitive impairment which was previously established with the CDR score for each case. When all the regions in the hippocampus were considered together, the correlation between density and CDR was statistically significant ( $r = 0.7964$ ,  $P < 0.0001$ ). Additionally, when each region was analyzed separately the densities of mAb AD2 immunoreactive intracellular-NFTs correlated significantly with the CDR value in CA3-CA2 ( $r = 0.7948$ ,  $P < 0.0001$ ), CA1-subiculum ( $r = 0.814$ ,  $P < 0.0001$ ) and in entorhinal cortex ( $r = 0.6979$ ,  $P = 0.0006$ ). The highest correlation was found in the frontal cortex ( $r = 0.8274$ ,  $P < 0.0001$ ).

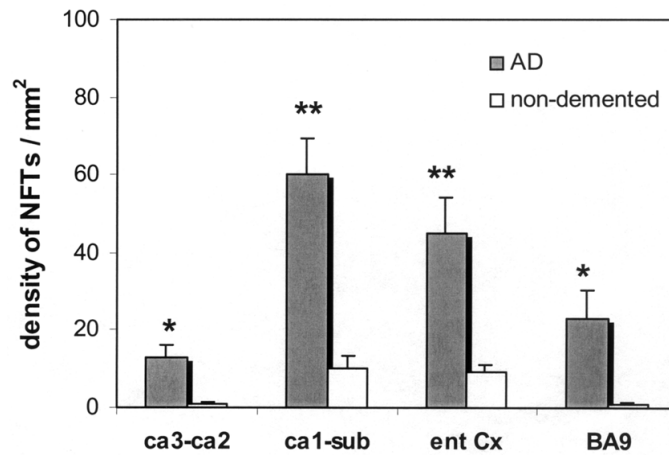


Fig. 4. Regional distribution of mAb AD2 immunoreactive NFTs in demented and non-demented groups. Three regions in the hippocampus (CA3-CA2, CA1-subiculum and entorhinal cortex) and one in the frontal lobe (BA9) were assessed. Density of NFTs corresponded to the average of 10 AD-cases and 10 non-demented cases. NFTs counts were performed using a 20x objective. Error bars represent standard error of the mean (SEM). For each region the statistical significance of the differences between density of NFTs for AD and non-demented groups was \* $P < 0.01$  for CA3-CA2 and BA9, and \*\* $P < 0.001$  in CA1-subiculum and entorhinal cortex areas.

#### 4. Discussion

The present study focused on the spatio-temporal formation of neurofibrillary changes that occur in normal aging and AD [2,5,17]. The study was performed using mAb AD2, an antibody that detects a phosphorylated epitope of the tau protein which is generated by phosphorylation of Ser396 and Ser404 residues [11]. Our quantitative study compared the changes in aging versus those observed in AD. Both in AD and non-demented cases, we found non-NFT bearing neurons which displayed a diffuse and granular AD2 immunoreactivity in the perinuclear area. Characteristically, these amorphous deposits were undetected by TR in the red channel (Figs 1(b) and 3(B)) suggesting a non-fibrillar state of such deposits. In addition, both in control and AD cases, these AD2 immunoreactive deposits were frequently associated with membranous structures like nuclear envelope (Figs 1(a) and 3(A)) and lipofuscin granules (Figs 1(b) and 3(B)). These findings agree with previous reports which demonstrate close association of tau immunoreactivity and endogenous membranes such as mitochondria, rough endoplasmic reticulum and lipofuscin granules [7,20,29]. In general, we interpret these results as representing early stages of tau accumulation probably occurring membrane bound. In this regard, membranous support may act as a template for the nucleation of the phosphorylated tau leading to PHFs formation as is showed in Figs 1a and 3A. The finding of mAb AD2 immunoreactive deposits in a non-fibrillar state as demonstrated

with TR (Figs 1(b) and 3(B)), supports previous publications suggesting that abnormally phosphorylation of tau protein precedes NFTs formation [2,5]. According with this, the non-fibrillar AD2 immunoreactive deposits may correspond to Braak's group 1 [5] or stage 0 of Bancher's classification [2]. Our findings appear to contrast with Kimura et al., in which they report that phosphorylation at Thr231 and Ser396 occurs after PHF assembly [28], a result that could be due to the additional recognition of mAb AD2 of a phosphorylated site on Ser404 in the tau molecule.

In this confocal microscopical analysis we were able to distinguish subtypes of NFTs based upon their patterns of AD2 immunoreactivity and TR counterstaining. In this regard, a subpopulation of TR positive intracellular-NFTs displayed an AD2 immunoreactivity which was diffuse granular rather than fibrillar, and distributed along the surface of the TR positive tangle (see Figs 1(c) and 3(C)). The second subpopulation of TR positive intracellular-NFTs was characterized by a clear colocalization between AD2 immunoreactivity and TR (Fig. 2(a)). This type of intracellular-NFT appeared green-yellow in the merged image (see Fig. 3(D)). Following Braak classification of NFT [5] the first population of structures characterized by diffuse granular mAb AD2 immunoreactivity (Figs 1(c) and 3(C)) would correspond to Group 2, while the second population (Figs 2(a) and 3(D)) to Group 3. As the AD cases used in our study were classified with moderate to severe dementia we expected to find mainly Group 3 mAb AD2 immunore-

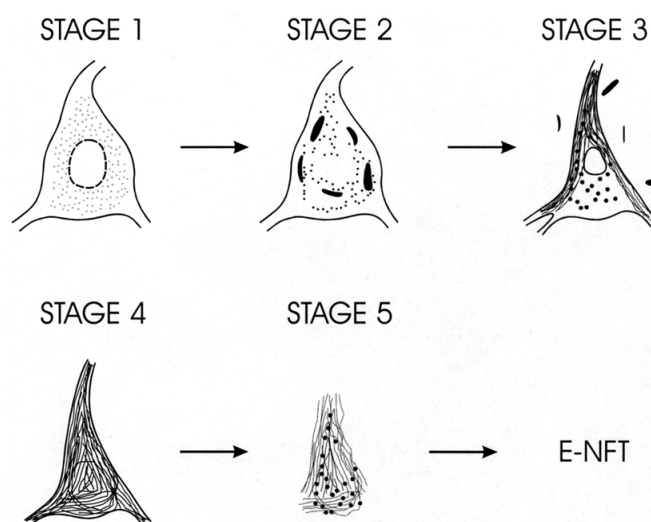


Fig. 5. Schematic drawing summarizing stages of mAb AD2 immunoreactivity in tangles. Stage 1 (pre-tangle stage I) corresponds to perinuclear and diffuse AD2 immunoreactivity which is generally undetected by TR. Stage 2 is characterized by amorphous granular mAb AD2 immunoreactivity located throughout the cytoplasm (pre-tangle stage II). TR fails to detect this stage. Stage 3 was characterized by granular AD2 immunoreactivity distributed along the intracellular tangle which is detected by TR. (tangle stage I). Stage 4. The typical intracellular tangle with fibrillar appearance is double labeled with AD2 and TR (tangle stage II). Stage 5 corresponds to a transitional stage in which the intracellular-NFT has become extracellular but still displays a coarse and sparse granular AD2 immunoreactivity (E-NFT stage I). Eventually the "ghost" tangle lacks antigenicity for mAb AD2 (E-NFT stage II).

active intracellular-NFTs. In general, the amount of the Group 2 intracellular-NFT was lower than Group 3 intracellular-NFTs. This observation is consistent with Group 2 intracellular-NFTs preceding Group 3.

A scheme of the staging of NFT formation based upon AD2 immunoreactivity and TR counterstaining is illustrated in Fig. 5. According with this, stage 1 corresponds to the structure illustrated in Fig. 3(A) and characterized by AD2 (+) immunoreactivity of perinuclear and diffuse appearance and TR (-). Stage 2 (illustrated in Fig. 3(B)) is characterized by dense AD2 (+) immunoreactivity TR (-) widespread in the perinuclear area and the cytoplasm. These states would correspond to "pre-tangle" stages. Stage 3 (illustrated in Fig. 3(C)) is characterized by either AD2 (+) of granular appearance and TR (+). Stage 4, intracellular-NFT is shown in Fig. 3(D) and characterized by full colocalization AD2 (+) and TR (+). The last stage 5 (illustrated in Fig. 3(E)) may correspond to Group 4 from Braak's classification [5]. This stage 5 tangle was characterized by an AD2 immunoreactivity similar to that present in stage 3 NFT formation, i.e. granular appearance rather than fibrillar. As the immunoreactivity to phospho-dependent antibody AD2 present on extracellular-NFTs is not possible to originate in the extracellular space, it may result from gradual proteolysis of the AD2 antigen in the transition of the intracellular-NFT to the extracel-

lular space to become an extracellular-NFT. Eventually, as shown in Fig. 3(E) (thick arrow) AD2 immunoreactivity would be lost in mature extracellular-NFTs. As it has been previously demonstrated, this structure will immunoreact with antibodies against ubiquitin [33] or truncated tau protein [29]. Furthermore, TR binding sites are also lost in the later stages of NFT degradation [30]. Similar stages of NFT formation as we illustrate in Fig. 5 have been recently described using a variety of immunological markers which identify PHF-associated tau protein [8,12,20,24]. All these reports provide evidences that intracellular-NFTs develop to extracellular-NFTs and that these lesions are in part related to neuronal death.

MAb AD2 labels PHFs at the electron microscopic level [35] and PHF-tau on immunoblots, allowing us to use it to define the biochemical pathway of neurofibrillary degeneration both in normal aging and AD [14]. Here, we analyzed the distribution and density of mAb AD2 immunoreactive intracellular-NFTs. The morphometric analysis evidenced differences between non demented aged cases and AD, related to the regional distribution and density of intracellular-NFTs found. As Fig. 4 shows, in AD cases intracellular-NFTs were found in high amount throughout the hippocampus, entorhinal cortex and frontal cortex, therefore we believe that measurements of mAb AD2 tangles densities could

be a suitable parameter to differentiate AD from non-demented cases.

On the other hand, it is generally accepted that the relationship between cognitive dysfunction and neurofibrillary degeneration is established only when they occur in the neocortex [1,3,15,16]. However, some studies have shown correlation between the density of neurofibrillary structures and the cognitive impairment in the hippocampus as it is shown in this paper [20,21,24]. We studied the relationship between the density of AD2 immunoreactive NFTs and cognitive status as defined by the CDR score. We found the highest correlation in the BA9 ( $r = 0.8274$ ,  $P < 0.0001$ ) and CA1-subiculum ( $r = 0.814$ ,  $P < 0.0001$ ) areas. Likewise, in CA3-CA2 and entorhinal cortical regions the density of intracellular-NFTs also correlated significantly with the CDR. These findings provides evidences that the increment in the density of mAb AD2 intracellular-NFTs in the hippocampus also influences cognitive impairment in AD. Taken all these data together, we can conclude that the extent of neurofibrillary changes both in the hippocampal and in the polymodal association neocortical areas, correlate well with cognitive impairment. However, these findings do not exclude the possibility that other mechanisms different to NFT formation may be involved in neuronal degeneration and death observed in vulnerable regions like hippocampus during AD.

In conclusion, our result provide evidence for the sequence of tangle formation as detected by mAb AD2. Our observations suggest that this process is characterized by a number of serial discrete stages. In addition, mAb AD2 immunoreactive intracellular-NFTs occurs in normal aged people, however, in significantly lower amounts than in AD cases and mainly distributed in entorhinal cortex and CA1-subicular regions. This study also indicates that the increase in the number of mAb AD2 immunoreactive intracellular-NFTs in susceptible regions, is related closely to the severity of dementia in AD. Finally, these findings demonstrate the value of the combination of accurate immunological markers with TR in confocal microscopy to understand the complex tau pathological processing leading to the PHFs assembly in AD and the disruption of neuronal networks.

### Acknowledgements

This work was supported by a grant from CONACyT-26319M (México) to R.M. We thank Dr. George Perry

for the critical reading and English editing of the manuscript and Ignacio Arauz for the drawing. MGv received financial support from CONACyT (México).

### References

- [1] P. Arriagada, J. Growdon, Hedley-Whyte and B. Hyman, Neurofibrillary tangles but not senile plaques parallel duration and severity of Alzheimer's disease, *Ann Neurol* **42** (1992), 631–639.
- [2] C. Baner, C. Brunner, H. Lassman, H. Budka, K. Jellinger, G. Wich, F. Seitelberger, I. Grundke-Iqbal and H. Wisniewski, Accumulation of abnormally phosphorylated  $\tau$  precedes the formation of neurofibrillary tangles in Alzheimer's disease, *Brain Res* **477** (1989), 90–99.
- [3] L. Bierer, P. Hof, D. Purohit, L. Carlin, J. Schmeidler, K. Davis and D. Perl, Neocortical neurofibrillary tangles correlate with dementia severity in Alzheimer's disease, *Arch Neurol* **52** (1995), 81–88.
- [4] M. Billingsley and R. Kincaid, Regulated phosphorylation and dephosphorylation of tau protein: effects on microtubule interaction, intracellular trafficking and neurodegeneration, *Biochem J* **323** (1997), 577–591.
- [5] E. Braak, H. Braak and E. Mandelkow, A sequence of cytoskeleton changes related to the formation of neurofibrillary tangles and neuropil threads, *Acta Neuropathol* **87** (1994), 554–567.
- [6] H. Braak and E. Braak, Neuropathological staging of Alzheimer-related changes, *Acta Neuropathol* **82** (1991), 239–259.
- [7] W. Bondareff, S. Matsuyama and P. Dell'Albani, Production of paired helical filament, Tau-like proteins by PC12 cells: A model of neurofibrillary degeneration, *J Neurosci Res* **52** (1998), 498–504.
- [8] W. Bondareff, C. Harrington, C.M. Wischik, D. Hauser and M. Roth, Immunohistochemical staging of neurofibrillary degeneration in Alzheimer's disease, *J Neuropathol Exp Neurol* **53** (1994), 158–164.
- [9] W. Bondareff, C.M. Wischik, M. Novak, W. Amos, A. Klug and M. Roth, Molecular analysis of neurofibrillary degeneration in Alzheimer's disease: An immunohistochemical study, *Am J Pathol* **137** (1990), 711–723.
- [10] L. Buée and A. Delacourte, Comparative biochemistry of tau in progressive supranuclear palsy, corticobasal degeneration, FTDP-17 and Pick's disease, *Brain Pathol* **9** (1999), 681–693.
- [11] V. Buée-Scherer, O. Condamines, C. Mourtou-Gilles, R. Jakes, M. Goedert, B. Pau and A. Delacourte, AD2, a phosphorylation-dependent monoclonal antibody directed against tau proteins found in Alzheimer's disease, *Mol Brain Res* **39** (1996), 79–88.
- [12] P. Cras, M.A. Smith, P.L. Richey, S.L. Siedlak, P. Mulvihill and G. Perry, Extracellular neurofibrillary tangles reflect neuronal loss and provide further evidence of extensive protein cross-linking in Alzheimer disease, *Acta Neuropathol* **89** (1995), 291–295.
- [13] A. Delacourte and A. Défossez, Alzheimer's disease: tau proteins, the promoting factors of microtubule assembly, are major components of paired helical filaments, *J Neurol Sci* **76** (1986), 173–186.
- [14] A. Delacourte, J.P. David, N. Sergeant, L. Buée, A. Watzet, P. Vermersch, F. Ghazali, C. Fallet-Bianco, F. Pasquier, F. Lebert, H. Petit and C. Di Menza, The biochemical pathway of

- neurofibrillary degeneration in aging and Alzheimer's disease, *Neurology* **52** (1999), 1158–1165.
- [15] D. Dickson, H. Crystal, C. Benova, W. Honer, I. Vincent and P. Davies, Correlations of synaptic and pathological markers with cognition of the elderly, *Neurobiol Aging* **16** (1995), 285–304.
- [16] C. Duyckaerts, M. Bencic, Y. Grignon, T. Uchihara, Y. Piette and J. Hauw, Modeling the relation between neurofibrillary tangles and intellectual status, *Neurobiol Aging* **18** (1997), 267–273.
- [17] T. Duong, T. Doucette, N. Zidenberg, R. Jacobs and A. Scheibel, Microtubule-associated proteins tau and amyloid P component in Alzheimer's disease, *Brain Res* **603** (1993), 74–86.
- [18] R. Endoh, M. Ogawara, T. Iwatsubo, I. Nakano and H. Mori, Lack of the carboxyl terminal sequence of tau in ghost tangles of Alzheimer's disease, *Brain Res* **601** (1993), 164–172.
- [19] D. Evans, K. Rank, K. Bhattacharya, D. Thomsen, M. Gurney and S. Sharma, Tau phosphorylation at Ser-396 and Ser-404 by human recombinant tau protein kinase II inhibits tau's ability to promote microtubule assembly, *J Neurosci* **20** (2000), 3937–3946.
- [20] F. García-Sierra, J. Hauw, C. Duyckaerts, C.M. Wischick, J. Luna-Muñoz and R. Mena, The extent of neurofibrillary pathology in perforant pathway neurons is the key determinant of dementia in the very old, *Acta Neuropathol* **100** (2000), 29–35.
- [21] F. García-Sierra, C.M. Wischick, C.R. Harrington, J. Luna-Muñoz and R. Mena, Accumulation of C-terminally truncated tau protein associated with vulnerability of the perforant pathway in early stages of neurofibrillary pathology in Alzheimer's disease, *J Chem Neuroanat* (in press).
- [22] M. Goedert, M. Spillantini, N. Cairns and R. Crowther, Tau-proteins of Alzheimer paired helical filaments—abnormal phosphorylation of all six brain isoforms, *Neuron* **8** (1992), 159–168.
- [23] T. Gómez-Isla, L.J. Price, W.D. McKeel, C.J. Jr. Morris, H.J. Growdon and T.B. Hyman, Profound loss of layer II entorhinal cortex neurons occurs in very mild Alzheimer's disease, *J Neurosci* **16** (1996), 4491–4500.
- [24] T. Gómez-Isla, R. Hollister, H. West, S. Mui, J.H. Growdon, R.C. Petersen, J.E. Parisi and B.T. Hyman, Neuronal loss correlates with but exceeds neurofibrillary tangles in Alzheimer's disease, *Ann Neurol* **41** (1997), 17–24.
- [25] I. Grundke-Iqbal, K. Iqbal, Y. Tung, M. Zaidi, H. Wisniewski and L. Binder, Abnormal phosphorylation of the Map tau in Alzheimer cytoskeletal pathology, *Proc Natl Acad Sci USA* **83** (1986), 4913–4917.
- [26] P. Hof, L. Bierer, D. Perl, A. Delacourte, L. Buée, C. Bouras and J. Morrison, Evidence for early vulnerability of the medial and inferior aspects of the temporal lobe in an 82-year-old patient with preclinical signs of dementia—regional and laminar distribution of neurofibrillary tangles and senile plaques, *Arch Neurol* **49** (1992), 946–953.
- [27] C. Hughes, L. Berg, W. Danzinger, L. Coben and R. Martin, A new clinical scale for the staging of dementia, *Br J Psychiatry* **140** (1982), 566–572.
- [28] T. Kimura, T. Ono, J. Takamatsu, H. Yamamoto, K. Ikegami, A. Kondo, M. Hasegawa, Y. Ihara, E. Miyamoto and T. Miyakawa, Sequential changes of tau-site-specific phosphorylation during development of paired helical filaments, *Dementia* **7** (1996), 177–181.
- [29] R. Mena, P. Edwards, C. Harrington, E. Mukaetova-Ladinska and C.M. Wischick, Staging the pathological assembly of truncated tau protein into paired helical filaments in Alzheimer's disease, *Acta Neuropathol* **91** (1996), 633–641.
- [30] R. Mena, P. Edwards, O. Pérez-Olvera and C.M. Wischick, Monitoring pathological assembly of tau and  $\beta$ -amyloid proteins in Alzheimer's disease, *Acta Neuropathol* **89** (1995), 50–56.
- [31] M. Morishima-Kawashima, M. Hasegawa, K. Takio, M. Suzuki, H. Yoshida, K. Titani and Y. Ihara, Proline-directed and non-proline-directed phosphorylation of PHF-tau, *J Biol Chem* **270** (1995), 823–829.
- [32] M. Morishima-Kawashima, M. Hasegawa, K. Takio, M. Suzuki, H. Yoshida, A. Watanabe, K. Titani and Y. Ihara, Hyperphosphorylation of tau in PHF, *Neurobiol Aging* **16** (1995), 365–380.
- [33] M. Morishima-Kawashima and Y. Ihara, Posttranslational modifications of tau in paired helical filaments, *Dementia* **52** (1994), 282–288.
- [34] J. Price, J. Davis and D. Morrison, The distribution of tangles, plaques and related immunohistochemical markers in healthy aging and Alzheimer's disease, *Neurobiol Aging* **12** (1991), 195–312.
- [35] S. Reig, V. Buée-Scherrer, C. Mourton-Gilles, A. Défossez, A. Delacourte, J. Beauvillain and M. Mazzuca, Immunogold labeling of paired helical filaments and amyloid fibrils by specific monoclonal and polyclonal antibodies, *Acta Neuropathol* **90** (1995), 441–447.
- [36] J. Resch, G. Lehr and C. Wischick, Design and synthesis of a potential affinity/cleaving reagent for beta-pleated sheet protein structures, *Bioorganic and Med Chem Lett* **1** (1991), 519–522.
- [37] M. Tabaton, S. Cammarata, G. Mancardi, V. Manetto, L. Autilio-Gambetti, G. Perry and P. Gambetti, Ultrastructural localization of  $\beta$ -amyloid,  $\tau$ , and ubiquitin epitopes in extracellular neurofibrillary tangles, *Proc Natl Acad Sci USA* **91** (1991), 7787–7791.
- [38] D. Yilmazer-Hanke and J. Hanke, Progression of Alzheimer-related neuritic plaque pathology in the entorhinal region, perirhinal cortex and hippocampal formation, *Dementia and Geriatric Cognitive Disorders* **10** (1999), 70–76.